Dynamic Estimation of Spin Satellite From the Single-Station ISAR Image Sequence With the Hidden Markov Model

YEJIAN ZHOU
Zhejiang University of Technology, Hangzhou, China

SHAOPENG WEI
Xidian University, Xi'an, China

LEI ZHANG
Sun Yat-Sen University, Shenzhen, China

WENAN ZHANG
Zhejiang University of Technology, Hangzhou, China

YAN MA
Beijing Institute of Tracking Telementry and Telecommunication, Beijing, China

With the increasing of on-orbit satellites, target dynamic monitoring becomes more and more important in space situation awareness applications. Currently, there are some exploratory methods monitoring attitude-stabilized targets using various high-resolution remote sensing technologies. However, it is still a big challenge to achieve dynamic estimation of spin satellite with single sensor. Inspired by the existing matching based works, this article presents a dynamic estimation method of spin satellite using single-station inverse synthetic aperture radar (ISAR) images. When the angle accumulation is set to be a constant in each ISAR imaging period, the projection change of target structures in the long-term observation sequence is described with the hidden Markov model to build the mathematic expression of target on-orbit state. In this condition, target sequential attitude can be solved with Viterbi decoding algorithm even the azimuth scaling of each image is difficulty due to target spin motion. Then, combined with the radar observation geometry, target sequential attitude parameters are substituted into a spin parameter optimization, which is solved by particle swarm optimization algorithm. In the end, target instantaneous attitude vectors and spin speed are used to express its dynamic during the observation period. Simulation experiments of a typical spin spacecraft, Tiangong-I, confirm the feasibility of the proposed algorithm, and its superiority is also investigated by comparison with the existing work.

Manuscript received 24 November 2021; revised 9 February 2022; released for publication 28 March 2022. Date of publication 31 March 2022; date of current version 11 October 2022.

DOI. No. 10.1109/TAES.2022.3164015

Refereeing of this contribution was handled by A. Manikas.

This work was supported by the National Natural Sciences Foundation of China under Grant 62101494, and in part by the Shenzhen Science and Technology Program under Grant KQTD20190929172704911.

Authors€ addresses: Yejian Zhou and Wenan Zhang are with the College of Information Engineering, Zhejiang University of Technology, Hangzhou, 310023, China, E-mail: (zhouyejian25@163.com); Shaopeng Wei is with the National Laboratory of Radar Signal Processing, School of Electronic Engineering, Xidian University, Xi'an 710071, China, and also with the Collaborative Innovation Center of Information Sensing and Understanding, Xidian University, Xi'an 710071, China, E-mail: (spw xd@163.com); Lei Zhang is with the School of Electronics and Communication Engineering, Sun Yat-Sen University (Shenzhen Campus), Shenzhen 518100, China, E-mail: (zhanglei57@mail.sysu.edu.cn); Yan Ma is with the Beijing Institute of Tracking Telementry and Telecommunication, Beijing 100094, China, E-mail: (mayan888@sina.com). *(Corresponding authors: Yejian Zhou; Lei Zhang.)*

I. INTRODUCTION

Nowadays, dynamic estimation of on-orbit satellites plays a more and more important role in space applications, such as satellite fault maintenance. When a satellite is no longer controlled by the ground-based station, it will probably break away from the stable-attitude state and spin on the orbit, threatening the security of nearby satellites. In this case, the satellite dynamic parameters, such as instantaneous attitude and motion period, become essential information to directly support its awareness analysis. Therefore, the research on dynamic estimation of those satellites has received widespread attention in the past decades [1]–[12].

Up to now, a variety of approaches have been used for satellite monitoring according to the high-resolution observation from the ground. For example, the range residual of mounted corner reflectors is employed to estimate satellites spin period through fitting its measured sequence with the historical database. The feasibility of this sort of method has been verified in tasks of tracking two spin satellites, Ajisai and ENVISAT, organized by the international laser ranging service (ILRS) since 2007 [1]–[6]. Another typical method of satellite dynamic estimation is rotating target 3-D model to a certain attitude, and then matching the generated inverse synthetic aperture radar (ISAR) images with the measured one. But it needs the prior azimuth scaling information for the spin satellites [7]–[9]. Besides, there are also some works based on the ISAR projection imaging theory. When the synchronization among high-resolution imaging sensors is achieved, target spin parameters can be obtained through solving target projection feature equations according to multistation ISAR images or optical-and-radar images [13]–[19].

However, in the single-station ISAR observation scene, it seems still a big challenge to determine spin parameters without the help of the observation from other imaging sensors. On the other hand, some related works [8], [9], [16] have concluded that target attitude can be recovered from the single-station ISAR image if the view of projection imaging and target 3-D model are given. This conclusion holds on a prerequisite that we should have the scaling information of

ISAR images. But, when the target spins on the orbit, it is hard to perform the azimuth scaling because the effective rotation can not be calculated from radar line of sight (LOS) parameters [16]–[18].

In order to achieve the dynamic estimation of spin satellites with single ground-based ISAR equipment, target projection image features among an ISAR sequence are described with the hidden Markov model (HMM) in this work [20]–[23]. With the historical observation training, the best matching path of target attitude change is decoded through Viterbi algorithm. In this way, the sequential attitude is determined under continuous rotation constraint of imaging view, and the azimuth scaling difficulty of each image is overcome. With the radar LOS parameters of the ISAR sequence, this attitude parameter sequence is substituted into target spin optimization later. Using the particle swarm optimization (PSO) algorithm, dynamic parameters including target instantaneous attitude and spin speed are solved in the end.

Compared with the existing methods, the proposed dynamic estimation method has some innovations.

1) To the best of our knowledge, it is the first time that single-station ISAR images have been used to estimate the dynamic parameters of spin satellites. Compared with the multisensor and multistation imaging models [16]–[18], single-station ISAR observation can be achieved without the synchronization among ground-based sensors. Besides, in the view of resource allocation of a certain ground-based ISAR observation network, the single-station strategy for satellite monitoring is more economical on the utilization of both time and space resource.
2) Different from most matching-based works [7]–[9], the proposed algorithm provides a brand-new viewpoint of target dynamic estimation that an HMM is used to describe the target attitude change according to the observed projection features. To some degree, it expands the frame matching to the state transforming of the feature sequence. In this way, the dimension of parameter optimization is decreased by the sequential state decoding. As a result, the proposed algorithm avoids solving the complex high-dimension parameter estimation, and models target spin motion with the *priori* target structure information instead. Therefore, this method can be applied to most known satellite monitoring.

The rest of the article is organized as follows: Section II illustrates the ISAR sequential imaging geometry of the on-orbit satellite, and the accumulated imaging angle expression is also derived. Section III investigates how to build an HMM to decode target motion on the orbit, while Section IV introduces how to use the proposed model for spin parameter estimation in details. In Section V, the experiments demonstrate the feasibility and superiority of the proposed algorithm, and finally, Section VI concludes this article.

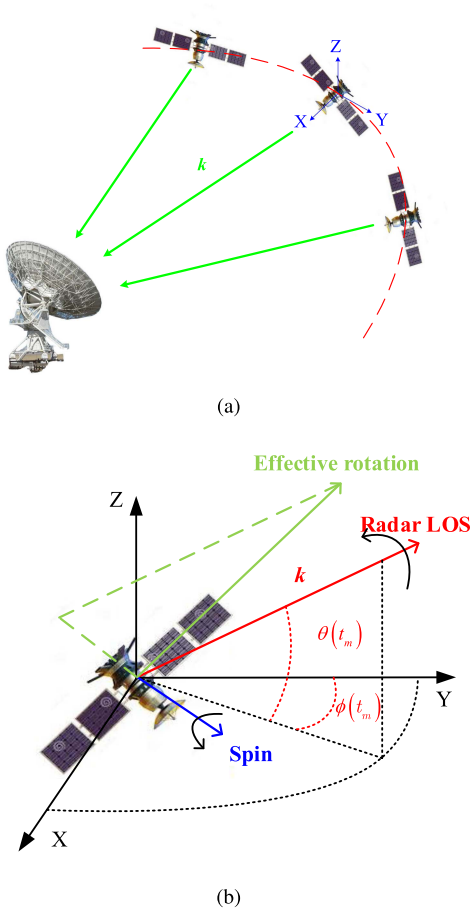

Fig. 1. Satellite target observation geometry. (a) Target observation geometry in 3-D world space. (b) Target observation geometry in the target Cartesian coordinate system.

II. SEQUENTIAL ISAR IMAGING FOR SPACE TARGET

As shown in Fig. 1(a), target on-orbit state is discussed in target Cartesian coordinate system, where the X-axis points to the earths core, the Y-axis is tangent to the objects orbit keeping in touch with object motion, and the Z-axis is the normal vector of object motion plane. During the full-lap radar observation, the ground-based radar line of sight (LOS) $\vec{\mathbf{k}}$ is described as the following equation [24], [25]:

$$\begin{aligned}&\vec{\mathbf{k}}\left(t_m\right)\\&=\left(\cos\theta\left(t_m\right)\sin\phi\left(t_m\right),\cos\theta\left(t_m\right)\cos\phi\left(t_m\right),\sin\theta\left(t_m\right)\right)^{\mathrm{T}}\end{aligned}\tag{1}$$

where t_m is slow-time related to the sampling of azimuth direction; the elevation angle $\theta(t_m)$ is the intersection angle between the instantaneous radar LOS vector and the XOY plane; and the azimuth angle $\phi(t_m)$ is the intersection angle between the Y-axis and the projection of the instantaneous radar LOS vector in XOY plane, shown in Fig. 1(b). In practical application, these LOS parameter sequences can be directly downloaded from radar tracking system.

Unlike optical imaging mechanism, the high-resolution ISAR imaging needs the coherent processing of the received

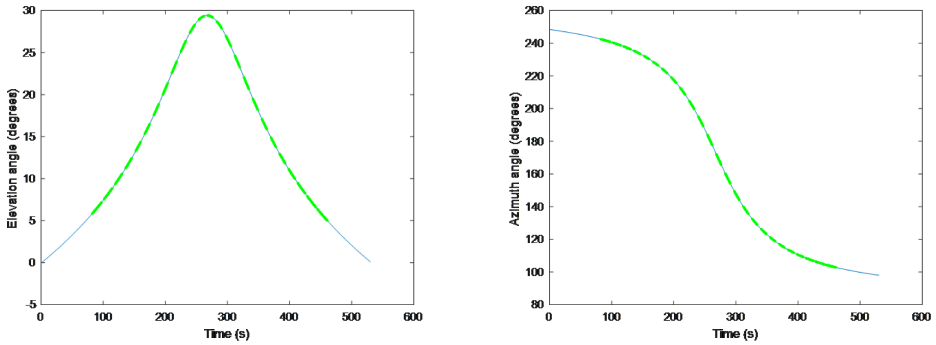

(a) (b)

Fig. 2. Echo segment strategy of single lap echo for similar angle accumulation. (a) Elevation angle sequence. (b) Azimuth angle sequence.

radar echo in both slow-time and fast-time domains, and its 2-D high resolutions are formed in different ways.

The range resolution, related to the echo accumulation in fast-time domain, depends on the band-wide of the transmit signal as follows:

$$\rho_r = \frac{\mathrm{c}}{2B} \tag{2}$$

where c is the speed of light, and B is the band wide of the transmit signal.

The azimuth resolution is based on the Doppler analysis of echo in slow-time domain. If the phase difference between two scattering points is more than 2π after the pulse accumulation [26], [27], the azimuth resolution is determined as

$$\rho_a = \frac{\lambda}{2\Delta\theta} \tag{3}$$

where λ is the wavelength of the transmit signal, and $\Delta\theta$ is the rotation angle in an ISAR imaging period.

In addition, we use the equal-angle accumulation principle to replace the conventional equal-time accumulation principle in the sequential ISAR imaging. During a single lap observation for a certain space target, the accumulated angle of each frame is a constant, as shown in Fig. 2.

With conventional range-Doppler (RD) imaging processing, we can calculate the accumulated angle $\vec{\mathbf{w}}_{\mathrm{LOS}}$ directly with the LOS parameters. In an imaging period, $\vec{\mathbf{w}}_{\mathrm{LOS}}$ is the intersection angle between the start LOS vector $\vec{\mathbf{k}}_1$, and the end LOS vector $\vec{\mathbf{k}}_2$, and its direction is determined by the right-hand rule

$$\vec{\mathbf{w}}_{\mathrm{LOS}} = \left\langle \vec{\mathbf{k}}_1, \vec{\mathbf{k}}_2 \right\rangle. \tag{4}$$

Then $\vec{\mathbf{w}}_{\mathrm{LOS}}$ can be directly used to achieve the azimuth scaling of ISAR image when the target has a stable attitude on the orbit. But for the spin targets, the contribution of target spinning also should be taken into consideration. As shown in Fig. 1(b), the effective accumulated angle $\vec{\mathbf{w}}_{\mathrm{eff}}$ in this case is calculated as

$$\vec{\mathbf{w}}_{\mathrm{eff}} = \vec{\mathbf{w}}_{\mathrm{LOS}} - \vec{\mathbf{w}}_{\mathrm{rot}} \tag{5}$$

$$\vec{\mathbf{w}}_{\mathrm{rot}} = (\cos\theta_{\mathrm{rot}} \sin\phi_{\mathrm{rot}}, \cos\theta_{\mathrm{rot}} \cos\phi_{\mathrm{rot}}, \sin\theta_{\mathrm{rot}})^{\mathrm{T}} \omega_{rot} T_{ac} \tag{6}$$

where θ_{rot} and ϕ_{rot} are the angle parameters of the spin shaft direction, which are defined in the same way as LOS parameters, ω_{rot} is the rotation speed, and T_{ac} is the accumulation time of the current imaging period.

III. IMAGING FEATURE EXPRESSION IN THE HMM

For most satellites, we use two angle parameters to build the attitude vector of a line-like structure as follows:

$$\vec{\mathbf{l}} = (\cos\alpha \sin\beta, \cos\alpha \cos\beta, \sin\alpha)^{\mathrm{T}} \tag{7}$$

where the attitude angle parameters of the typical structure α and β are defined in the similar way as LOS parameters.

According to the ISAR projection model in related works [24]–[27], RD imaging processing can be described as the projection of 3-D target coordinates onto the 2-D imaging plane. As long as the radar LOS parameters are given, target projection feature in the R-D image can be related to the target attitude vectors in the real 3-D space through the ISAR equivalent projection imaging equation.

In this way, the projected length of the structure in range direction of ISAR image is calculated as

$$r = L\vec{\mathbf{k}}_{\mathrm{C}} \bullet \vec{\mathbf{l}} \tag{8}$$

where $\bullet$ denotes the inner product, and $\vec{\mathbf{k}}_C$ is the center LOS vector of the imagery, L refers to the 3-D length of the typical structure.

Similarly, the projected length of the structure in azimuth direction of ISAR image is calculated as

$$\begin{aligned} d &= L\vec{\mathbf{fd}} \bullet \vec{\mathbf{l}} \\ &= \left|\vec{\mathbf{fd}} \bullet \vec{\mathbf{l}}\right| L\omega_{\mathrm{eff}} \sin\varphi \end{aligned} \tag{9}$$

$$\sin\varphi = \sqrt{1 - \left(\vec{\mathbf{fd}} \bullet \vec{\mathbf{l}}\right)^2} \tag{10}$$

where φ is the intersection angle between the rotation shaft and the attitude vector of the typical structure, $\vec{\mathbf{fd}}$ is the Doppler vector of the imagery which depends on the

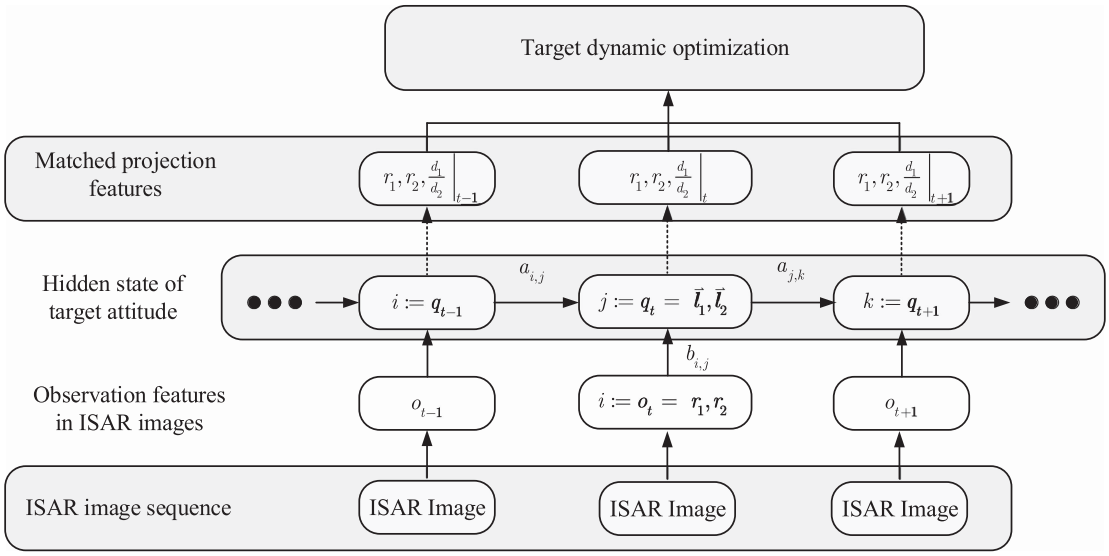

Fig. 3. Decoding of target attitude state sequence under the hidden Markov model.

effective rotation of radar LOS in the imaging period

$$\vec{\mathbf{fd}} = \frac{\vec{\mathbf{k}}_C \times \vec{\mathbf{w}}_{\text{eff}}}{\left\| \vec{\mathbf{k}}_C \times \vec{\mathbf{w}}_{\text{eff}} \right\|} \tag{11}$$

where $\times$ is the outer product of two vectors.

$\vec{\mathbf{k}}_C$ is easily determined in the scene of satellite ISAR observation, while the determination of $\vec{\mathbf{fd}}$ is more complicated. Because the calculation of $\vec{\mathbf{fd}}$ is coupled with target spin estimation when the target is not stabled on the orbit any more. Therefore, the azimuth-axis projected length of single structure is hard to be directly used in the target dynamic estimation.

On the other hand, for most satellites, their on-orbit attitude information can be described with the vectors $(\vec{\mathbf{l}}_1, \vec{\mathbf{l}}_2)$ of two perpendicular structures, for example, the body and solar wings of the TG-I. From previous works [7]–[9], one projection observation (r_1, r_2, d_1, d_2) is related to a certain attitude state described by $(\vec{\mathbf{l}}_1, \vec{\mathbf{l}}_2)$

$$\left(\vec{\mathbf{l}}_1, \vec{\mathbf{l}}_2\right) \rightarrow (r_1, r_2, d_1, d_2)\,. \tag{12}$$

That is to say, if we obtain projection observation values and attitude states in all observation angles, the attitude state in a certain observation angle can be determined through feature matching. This is also the key point of existing works of attitude matching for space targets, but some tricks should be added in the case of target dynamic estimation for spin satellites. First, image feature r can be easily measured from the observation ISAR image with known range resolution. Second, although the measurement of azimuth projection d is difficult to be achieved without the azimuth scaling, the projection length ratio of two structures helps the attitude matching and target spin estimation when the target 3-D model is given in advance. Therefore, it provides a potential approach to decouple the coupling of observation geometry scaling and target spin estimation when several images are jointly interpreted.

In this work, an HMM process is built to achieve target attitude state decoding from an equiangular ISAR image sequence based on target imaging projection feature. When the angle interval of ISAR imaging is about 3 degrees and the target spins at uniform speed (generally around 0.015 rad/s in practical), target attitude change in the ISAR image sequence can be expressed as the state transfer in a Markov hidden state sequence, as shown in Fig. 3

$$P\left(q_t = o_t | q_1 \cdots q_{t-1}\right) = P\left(q_t = o_t | q_{t-1}\right) \tag{13}$$

and the observation sequence $O = \{o_1, o_2, \ldots, o_T\}$ is collected according to the measured projection structure lengths in range dimensional of ISAR images.

$$o_t = \left(r_{1,t}, r_{2,t}\right). \tag{14}$$

For a certain cooperation target, the hidden states $Q = \{q_1 \cdots q_N\}$ of the projection structure lengths can be calculated in all potential LOS conditions according to (8). Before training the HMM with simulated observation sequences, the transition probability matrix for this Markov chain is initialized with Gaussian function as

$$a_{i,j} = p\left(q_i, q_j\right) = \frac{\exp\left(-\frac{\left\|q_i - q_j\right\|^2}{\sigma_1^2}\right)}{\sum_{j=i}^{N} \sum_{i=1}^{N-1} \exp\left(-\frac{\left\|q_i - q_j\right\|^2}{\sigma_1^2}\right)} \tag{15}$$

where the variance parameter σ_1^2 can be regulated to reflect the prior target attitude stability.

Taking the image feature extraction bias into the consideration of the sequence observation, the emission probability matrix is also initialized with a Gaussian

function as

$$b_{i,j} = p\left(o_i|q_j\right) = \frac{\exp\left(-\frac{\left\|o_i - q_j\right\|^2}{\sigma_2^2}\right)}{\sum_{j=i}^{N}\sum_{i=1}^{N-1}\exp\left(-\frac{\left\|o_i - q_j\right\|^2}{\sigma_2^2}\right)} \tag{16}$$

where the variance parameter σ_2^2 represents the tolerance of length extraction in the image.

Without the prior knowledge of the target initial attitude, the initial probability distribution over states $\prod = \{\pi_1, \pi_2, \ldots, \pi_N\}$ is uniform distribution

$$\pi_i = \frac{1}{N}. \tag{17}$$

After the training, the HMM is used to decode the observation sequence $O = \{o_1, o_2, \ldots, o_T\}$. Once the best path $Q_T{}^* = \{q_1{}^* \cdots q_T{}^*\}$ is obtained, the projected length of each structure in range axis is determined

$$q_t{}^* = \left(r_{1,t}{}^*, r_{2,t}{}^*\right). \tag{18}$$

For the hidden state $q_t{}^*$, the projected length of each structure in azimuth is still not ensured due to its uncertain motion. However, the projected length ratio of two structures should be calculable in each frame, which only depends on the geometry relationship between target instantaneous attitude and observation Doppler direction

$$\begin{aligned} f\left(\vec{\mathbf{l}}_1\vec{\mathbf{l}}_2\right) = \frac{d_1}{d_2} &= \frac{\left|\vec{\mathbf{fd}}\bullet\vec{\mathbf{l}}_1\right|L_1\omega_{\text{eff}}\sin\varphi_1}{\left|\vec{\mathbf{fd}}\bullet\vec{\mathbf{l}}_2\right|L_2\omega_{\text{eff}}\sin\varphi_2} \\ &= \frac{\left|\vec{\mathbf{fd}}\bullet\vec{\mathbf{l}}_1\right|L_1\sqrt{1-\left(\vec{\mathbf{fd}}\bullet\vec{\mathbf{l}}_1\right)^2}}{\left|\vec{\mathbf{fd}}\bullet\vec{\mathbf{l}}_2\right|L_2\sqrt{1-\left(\vec{\mathbf{fd}}\bullet\vec{\mathbf{l}}_2\right)^2}} \end{aligned} \tag{19}$$

$$\vec{\mathbf{fd}} = \frac{\vec{\mathbf{k}}_{C,i}\times\vec{\mathbf{w}}_{\text{eff,i}}\left(\vec{\mathbf{w}}_{\text{rot}}\right)}{\left\|\vec{\mathbf{k}}_{C,i}\times\vec{\mathbf{w}}_{\text{eff,i}}\left(\vec{\mathbf{w}}_{\text{rot}}\right)\right\|} \tag{20}$$

where $\bullet$ is the inner product of two vectors, and $\times$ is the outer product of two vectors.

That is to say, even the image scaling is not completed, this ratio measured from the observation parameters $(d_{1,t}, d_{2,t})$ provides the indirect attitude information. As shown in (21), it helps the attitude estimation through local searching in the feasible region Ω_1 determined by $(r_{1,t}{}^*, r_{2,t}{}^*)$

$$\left(\tilde{\vec{\mathbf{l}}}_1\tilde{\vec{\mathbf{l}}}_2\right) = \underset{\left(\vec{\mathbf{l}}_1\vec{\mathbf{l}}_2\right)\in\Omega_1}{\arg\min}\left|f\left(\vec{\mathbf{l}}_1\vec{\mathbf{l}}_2; r_{1,t}{}^*, r_{2,t}{}^*\right) - \frac{d_{1,t}}{d_{2,t}}\right|. \tag{21}$$

Once the attitude vectors of these two structures are obtained in each imaging period, the target spin parameters can be estimated in below optimization

$$\min_{\vec{\mathbf{w}}_{\text{rot}}}\sum_{t=1}^{T}\left|f\left(\vec{\mathbf{w}}_{\text{rot}}, t\right) - \frac{d_{1,t}}{d_{2,t}}\right|. \tag{22}$$

Besides, with estimated parameters $(\theta_{\text{rot}}, \phi_{\text{rot}}, \omega_{\text{rot}})$, the azimuth scaling of each ISAR image is also achieved as a by-product.

IV. TARGET STATE ESTIMATION WITH ISAR IMAGE SEQUENCE

The proposed target state estimation framework comprises three components: HMM training with simulated dataset, observation sequence decoding, and target parameter estimation. The flow of the proposed method is depicted in Fig. 4, and the details are as follows:

1) *Step 1*: According to radar LOS sequence, the whole lap of ISAR echo is divided into several segments. Each segment has the same angle accumulation and is processed with RD imaging algorithm.
2) *Step 2*: According to (4), the accumulated angle $\vec{\mathbf{w}}_{\text{LOS}}$ of each image is calculated with the LOS parameters.
3) *Step 3*: The target projection lengths of two structures in range and Doppler dimensions $(\hat{r}_{1,t}, \hat{d}_{1,t}, \hat{r}_{2,t}, \hat{d}_{2,t})$ are extracted from each image, and the observation value $o_t = (\hat{r}_{1,t}, \hat{r}_{2,t})$ is also obtained.
4) *Step 4*: With the trained HMM parameters $\lambda = (A, B, \prod)$, Viterbi algorithm is adopted to search the best solution of hidden state sequence $Q_T{}^* = \{q_1{}^*, \ldots, q_T{}^*\}$ of the observation sequence $O = \{o_1, o_2, \ldots, o_T\}$.
5) *Step 5*: For the obtained state $q_t{}^* = (r_{1,t}{}^*, r_{2,t}{}^*)$, the feasible region of target instantaneous attitude is established in each frame. Then, the observation of Doppler-dimensional projection lengths $(d_{1,t}, d_{2,t})$ and the radar LOS sequences are substituted into (21). And local searching method is adopted to solve target attitude, which will be converted into target Cartesian coordinates later.
6) *Step 6*: In the end, according to the obtained target attitude sequence, the PSO algorithm is used to estimate the target spin estimation in (22). Once the spin parameters $(\theta_{\text{rot}}, \phi_{\text{rot}}, \omega_{\text{rot}})$ are determined, the azimuth scaling of whole image sequences also can be achieved.

A. Dataset Simulated and Image Feature Extraction

As this article focuses on the state monitoring for cooperative target, target 3-D model is acquired in advance. It means that target ISAR image can be easily simulated when LOS parameters are calculated in some satellite orbit simulation tools, like satellite tool kit. If the observation sequence has the same observation interval and similar image resolution (corresponding to the equal-angle accumulation in the imaging period), all-view ISAR imaging simulation can be used to build the observation dataset through spherical sampling. In order to describe targets attitude change precisely in the sequence, the sampling interval should be no more than the average of the rotation angle between adjacent ISAR images in the all-lap observation.

On the other hand, the target state estimation is based on the target projection feature in ISAR imagery in this

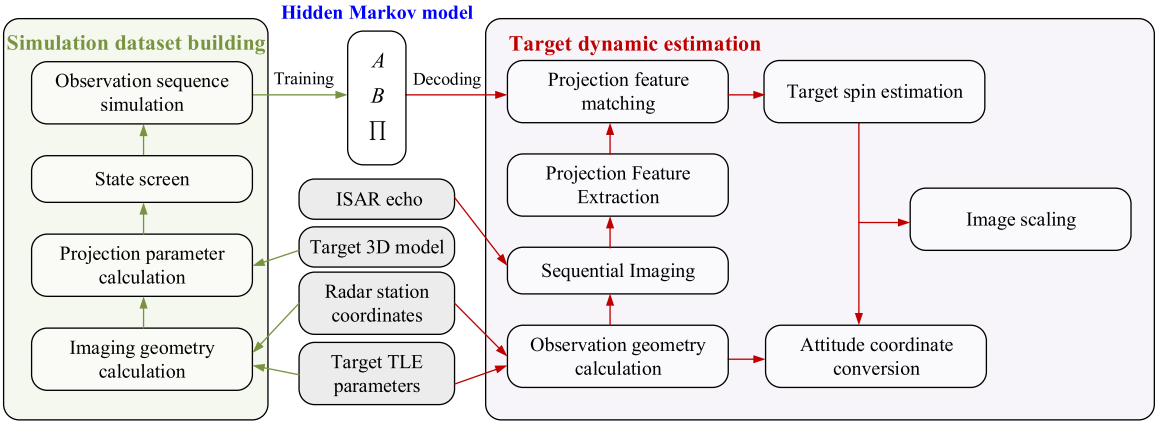

Fig. 4. Flowchart of the proposed algorithm.

article. The feature is used to build the HMM for decoding the observation values. The image feature extraction in the observation sequence can be achieved in both manually or automatically [28], [29], but the extraction bias ought to be taken into consideration. Empirically, when projection length of the structure is less than 10 pixels in the imagery, the proposed parameter estimation method fails even the extraction bias of target projection feature is three-pixel level. Under this principle, a large of target attitude state should be deleted in the simulation dataset according to (7)–(9), and the number of target potential state also sharply decreases in the HMM.

B. Multiple Observation Training From Simulated Dataset

As the target attitude change in an observation sequence can be described with the Markov process, a HMM is built to decode its hidden attitude state with the previous extracted image feature. In the classical decoding algorithm, transition probability matrix and emission probability matrix are *priori*. Therefore, it is necessary that the simulated observation sequences obtained in the different radar LOS sequence and similar target spin parameters are used to train these two matrices. The extracted projection lengths of these two perpendicular structures are defined as the state observation in each image

$$o = (r_1, r_2)\,. \tag{23}$$

In order to train the transition probability matrix and emission probability matrix from the observation samples, the Baum–Welch algorithm is refined with multiple observation trick [30], [31]. The multiple observation of radar feature is expressed as

$$\mathbf{O} = \left\{O^{(1)}, O^{(2)}, \ldots, O^{(K)}\right\} \tag{24}$$

where $O^{(k)} = \{o_1^{(k)}, o_2^{(k)}, \ldots, o_T^{(k)}\}$ is the individual observation sequence.

As each observation is independent from each other, the observation probability is as follows:

$$P(\mathbf{O}|\lambda) = \prod_{k=1}^{K} P(O^{(k)}|\lambda). \tag{25}$$

Herein, the state transition probability and symbol emission probability in the conventional maximization step are rewritten as

$$\bar{a}_{ij} = \frac{\sum_{k=1}^{K}\sum_{t=1}^{T_k-1}\xi_t^{(k)}(i,j)}{\sum_{k=1}^{K}\sum_{t=1}^{T_k-1}\gamma_t^{(k)}(i)} \tag{26}$$

$$\bar{b}_j(m) = \frac{\sum_{k=1}^{K}\sum_{t=1,o_t^{(k)}=v_m}^{T}\gamma_t^{(k)}(j)}{\sum_{k=1}^{K}\sum_{t=1}^{T}\gamma_t^{(k)}(j)} \tag{27}$$

where the expected state transition count $\xi_t^{(k)}(i,j)$ represents the probability of being in state q_i at time t and state q_j at time $t+1$ given the observation sequence $O^{(k)}$ yielding

$$\begin{aligned}\xi_t^{(k)}(i,j) &= P\left(q_t = q_i, q_{t+1} = q_j|O^{(k)}, \lambda\right)\\ &= \frac{\alpha_t(i)a_{ij}b_j\left(O_t^{(k)}\right)\beta_{t+1}(j)}{P\left(O^{(k)}|\lambda\right)}.\end{aligned} \tag{28}$$

And the expected state occupancy count $\gamma_t^{(k)}(j)$ represents the probability of being in state q_j at time t given the observation sequence $O^{(k)}$ yielding

$$\begin{aligned}\gamma_t^{(k)}(j) &= P\left(q_t = q_j|O^{(k)}, \lambda\right)\\ &= \sum_{i=1}^{N}\xi_t^{(k)}(i,j)\end{aligned} \tag{29}$$

where forward probability $\alpha_t(i)$ and backward probability $\beta_{t+1}(j)$ still can be calculated inductively.

Comprising the expectation step (E-step) and the maximization step (M-step), a brief flow of the training algorithm is given as follows:

1) *Step 1*: Initialize the transition probability matrix and emission probability matrix, and the initial state

probability is calculated as

$$\bar{\pi}_i = \frac{1}{K}\sum_{k=1}^{K}\gamma_1^{(k)}(i) \tag{30}$$

$$\alpha_1(i) = \pi_i b_i\left(o_1^{(1)}\right) \tag{31}$$

$$\beta_T(j) = 1. \tag{32}$$

And also input the multiple observation $\mathbf{O} = \{O^{(1)}, O^{(2)}, \ldots, O^{(K)}\}$, the maximum number of iteration and the minimum update movement.

2) *Step 2*: Calculate the observation even probability parameters of the current expectation step, $\xi_t^{(k)}(i, j)$ and $\gamma_t^{(k)}(j)$ according to (25), (28), and (29).
3) *Step 3*: Update the state transition probability and symbol emission probability after the maximization processing according to (26) and (27).
4) *Step 4*: If the maximum number or minimum move criterion of iteration is satisfied, break up the current iteration and turn to output current estimation results of the transition probability matrix **A** and emission probability matrix **B**; otherwise, turn to Step 2.

As mentioned in Section III, from the previous experience, it is acceptable that Gaussian function is used to initialize the transition probability matrix and emission probability matrix in the real application.

C. Target State Decoding With the Measured Sequence

Once the transition probability matrix **A** and emission probability matrix **B** are determined, the classical Viterbi algorithm is used to search the best solution of hidden state sequence $Q_T{}^* = \{q_1{}^* \cdots q_T{}^*\}$ [22]. As one of the dynamic programming methods, it can recursively search the state path with the highest probability, and the flow of this algorithm is briefly given as follows.

1) *Step 1*: Calculate the initial state $v_1(j) = \pi_j b_j(o_1)$, and determine the best step $q_1^* = \arg\max_{j=1}^{N}\pi_j b_j$.
2) *Step 2*: Calculate the Viterbi path probability at time t $v_t(j) = \max_{i=1}^{N} v_{t-1}(i)a_{ij}b_j(o_t)$, and determine the best step $q_t^* = \arg\max_{i=1}^{N} v_{t-1}(i)a_{ij}b_j(o_t)$.
3) *Step 3*: Update the best path $Q_t{}^* = \{q_1{}^* \cdots q_t{}^*\}$. If the iteration $t = T$, break up the current iteration and turn to Step 4; otherwise, turn to Step 2.
4) *Step 4*: Output the best path $Q_T{}^* = \{q_1{}^* \cdots q_T{}^*\}$.

D. Target State Estimation With PSO Algorithm

After the target hidden state decoding, the projected length ratio of two structures is matched with that in the simulated dataset to determine the target attitude in each frame. Then, LOS parameters in each imaging period and the attitude vectors of these two structures are substituted into target spin optimization (22). In this article, the classical PSO algorithm is used to solve this optimization [32], [33], and the fitness function is defined as

$$J = \sum_{t=1}^{T}\left| f\left(\vec{\mathbf{w}}_{\text{rot}}, t\right) - \frac{d_{1,t}}{d_{2,t}}\right|. \tag{33}$$

The solution is defined as the particle position.

$$X_i = (\theta_{\text{rot}}, \phi_{\text{rot}}, \omega_{\text{rot}})^T. \tag{34}$$

With the swarm search and particle search experience in the former iteration, the particle's position and velocity are updated by the following rules:

$$V_i(t+1) = a_0 V_i(t) + a_1 \text{rand}_1\left(pBest - X_i(t)\right) + a_2 \text{rand}_2\left(\text{GBest} - X_i(t)\right) \tag{35}$$

$$X_i(t+1) = X_i(t) + V_i(t) \tag{36}$$

where Gbest is the best swarm position, and Pbest is the best particle position.

A brief flow of PSO is given as follows.

1) *Step 1*: Input the maximum iteration and minimum move distance of the optimization. Randomly sample in the solution space to form a particle swarm.
2) *Step 2*: Determine the Gbest and Pbest according to the fitness function (33) in the current swarm.
3) *Step 3*: Update the position and velocity of each particle according to (35)–(36), and rebuild the swarm position.
4) *Step 4*: Search the Gbest and Pbest in the generated swarm, and calculate the move distance between the current and former swarm. If the maximum iterations or minimum move criterion is satisfied, break up the current iteration and turn to Step 5; otherwise, turn to Step 3.
5) *Step 5*: Output the position of the ideal particle.

In the end, with estimated parameters $(\theta_{\text{rot}}, \phi_{\text{rot}}, \omega_{\text{rot}})$, the azimuth information of each ISAR image is easily scaled with LOS parameters according to (4)–(6), and target instantaneous attitude also will be determined in target Cartesian coordinate system.

V. EXPERIMENT ANALYSIS

In this section, the proposed algorithm will be investigated in the simulation experiments. In these experiments, a typical satellite, TG-I is used for the simulation. the body and solar wing of the satellite are perpendicular, which are adopted as the feature structures in the later processing, as shown in Fig. 5.

In the first experiment, the feasibility of the proposed algorithm is investigated with an ISAR image sequence of a 400-km-altitude spin target. In the second part, the steadiness performance of the proposed algorithm is investigated in different observation and feature extraction conditions. In the end, the estimation results of the proposed algorithm are compared with those of the method in [27] to illustrate its progress on handling dynamic estimation of spin targets.

Acquisition of Observed ISAR Image Sequence: Due to lacking real measured ISAR data, the observed ISAR echo is simulated by using the improved physical optical

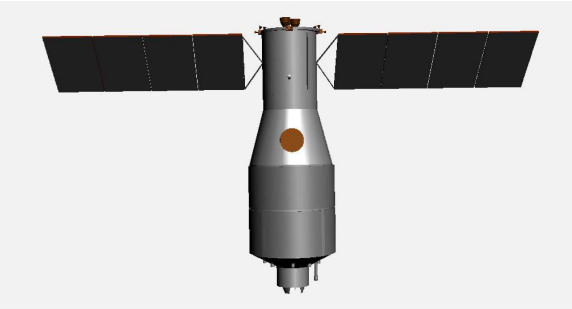

Fig. 5. 3-D model of TG-I.

TABLE I
Main Parameters of Isar System

Size of Images	256 × 512
Wave Length of the Signal	0.018 m
Bandwidth	600 MHz
Sample Frequency	1.2 GHz
Center Frequency of Transmit Signal	16.7 GHz
Pulse Repetition Frequency	100 Hz

algorithm [34]–[36]. The main parameters of the ISAR system are given in Table I. The location coordinates of the ground-based observation stations and target two-line-element (TLE) parameters are used to build the whole observation scene. Then the conventional range-Doppler imaging algorithm is adopted to process the obtained echo for generating six ISAR images in each observation sequence with the segment principle mentioned in Section II.

Acquisition of Image Feature Dataset: The target image feature dataset is built with the static target in the scene, where the radar LOS vectors are spherically sampled and the image azimuth rotates around the certain LOS vector. Both the sampling and rotation interval are 2 degrees. As mentioned in Section IV, the observation where the projection length of any structure is less than 10 pixels is deleted later.

A. Demonstration Experiment

Before the target dynamic parameter estimation, more than 300 image feature sequences are generated to train the HMM in the two different target scenes. The ground station is located at Beijing (39.9 N, 116.4 E, 66 m) and two sets of 400-km-altitude TLE parameters are adopted to calculate target trajectory. Besides, the target spin speed of these samples ranges from 0.010 to 0.018 rad/s according to the published measurement results [1], [2], [16]. Then, another observation image sequence is generated in the condition that the target spins at 0.015 rad/s around a fixed shaft. The projection lengths are extracted as shown in the first row of Fig. 6. With the obtained HMM parameters, the attitude state in this observation sequence is decoded according to (21). A visional comparison of the matching result is also given between the first row and second row of Fig. 6, which reflects the feasibility of the proposed target attitude sequence matching method using Viterbi decoding.

Then, the matched image feature are substituted into optimization (22) to estimate target spin parameters. By using PSO algorithm, the estimation results are obtained, shown in Table II. With these motion information, the target instantaneous attitude vector in each frame also can be calculated under target Cartesian coordinate system after the LOS parameters are substituted into (4)–(6). The numeric comparisons in Table II prove the feasibility of the proposed algorithm. When the observation ISAR image sequence is correctly matched with the simulated imagery, the estimated spin parameters are close to the true value and the estimation error of each target instantaneous attitude vector is below 3 degrees.

B. Expansion Experiments in Different Observation Conditions

Furthermore, in order to investigate the capability of the proposed algorithm in the practical application, two experiments are designed. In these two experiments, the altitude of target orbit is near to 400 km.

In the first additional experiment, two sets of TLE parameters are used to build the observation geometry and the parameters of target spin motion are also different from the former. The image projection feature extraction results are depicted in the first row of Figs. 7 and 8, respectively. By the Viterbi algorithm, these images are matched with those in the simulated dataset according to the trained HMM in Section V-A. Similarly, the matching results of three frames in the observation are also given in the second row of Figs. 7 and 8, respectively. The dynamic estimation results in Table III confirm the feasibility of the proposed algorithm in different observation conditions. It should be emphasized that the observation conditions of these two scenes are still close to that of trained samples, where the altitude of target orbit is near to 400 km. For other cases, the HMM parameters needs to be retrained as the accuracy of image feature matching is the premise of target dynamic parameter estimation in this work.

In the second experiment, the repetition experiments are made in different extraction bias of image feature, which affects the matching performance of attitude sequence directly. It is repeated 20 times in each extraction condition, and the averaged initial attitude vectors of these two structures are chosen to reflect the performance of the proposed algorithm. As shown in Fig. 9, even if there is a extraction bias of 8 pixels in the ISAR images of TG-1, the attitude estimation error of its body and solar wing still can be kept under 10 degrees. The robustness of the proposed method is confirmed. In other words, the accuracy of the spin parameter estimation is ensured when this bias is not over 6 pixels, which can be easily achieved in the most real applications.

C. Comparison Experiments With Existing Work

In order to illustrate the advantage of the proposed algorithm on using single-station ISAR observation image, the performance of the proposed method is compared with

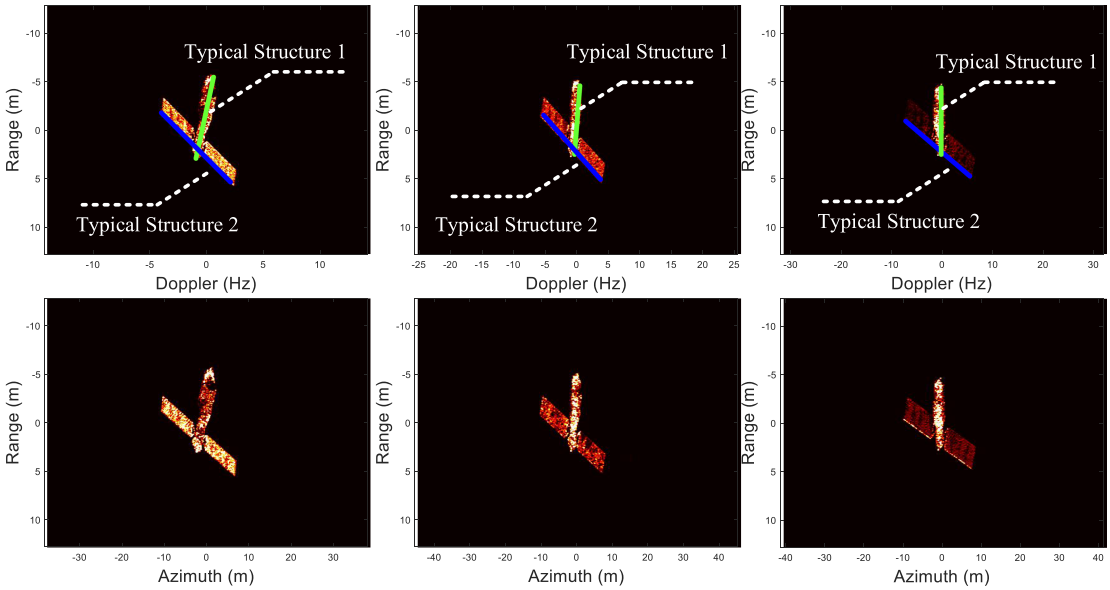

Fig. 6. Observation image feature extraction and matching with the simulation dataset. (First row: Feature extraction results of three frames in the observation image sequence; Second row: Image matching results with the simulation dataset via HMM decoding.).

TABLE II
Target Dynamic Estimation Results of Tg-I

Parameter	True value	Estimation result	Error
The direction vector of the structure 1 in frame 1	(0.2903,-0.6294,0.7208)	(-0.3079,0.6197,-0.7219)	1.16 degrees
The direction vector of the structure 2 in frame 1	(-0.1535,0.7129,0.6843)	(-0.1490,0.7180,0.6799)	0.46 degrees
The direction vector of the structure 1 in frame 3	(-0.0562,-0.1247,0.9906)	(-0.0531,0.3056,-0.9507)	1.06 degrees
The direction vector of the structure 2 in frame 3	(0.0925,0.9873,0.1295)	(-0.0046,0.9519,0.3063)	0.37 degrees
The direction vector of the structure 1 in frame 5	(-0.1232,0.0642,0.9903)	(0.1078,-0.0667,-0.9919)	0.90 degrees
The direction vector of the structure 2 in frame 5	(0.1995,0.9791,-0.0387)	(0.2009,0.9786,-0.0440)	0.31 degrees
The direction vector of the spin shaft	(-0.6428,0.7660,0)	(-0.6658,0.7448,-0.0440)	3.10 degrees
Target spin speed	0.013 rad/s	0.013 rad/s	0

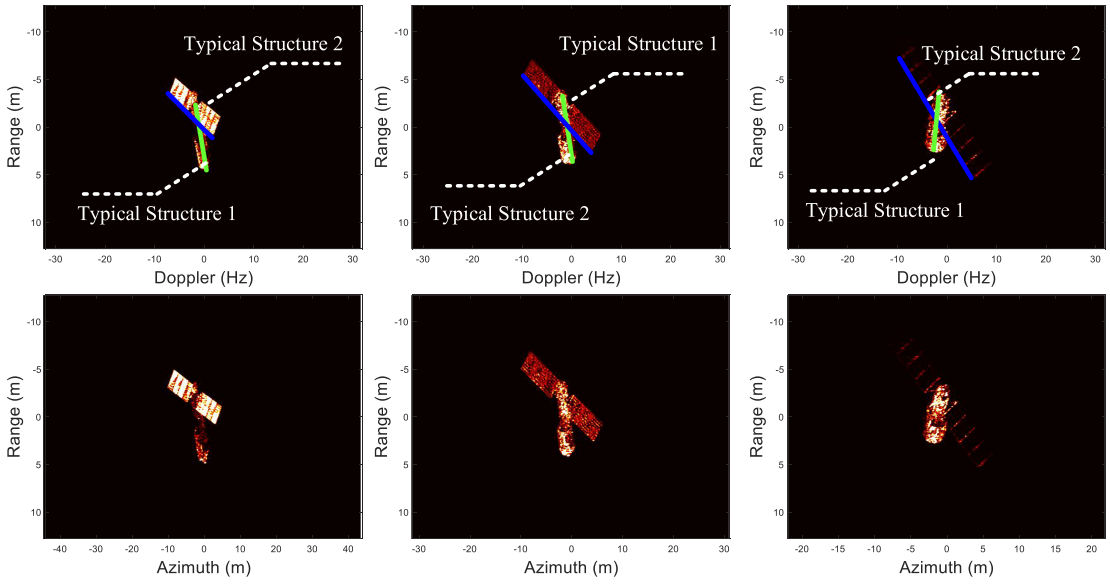

Fig. 7. Observation image feature extraction and matching with the simulation dataset in Scene 1. (First row: Feature extraction results of three frames in the observation image sequence; Second row: Image matching results with the simulation dataset via HMM decoding.).

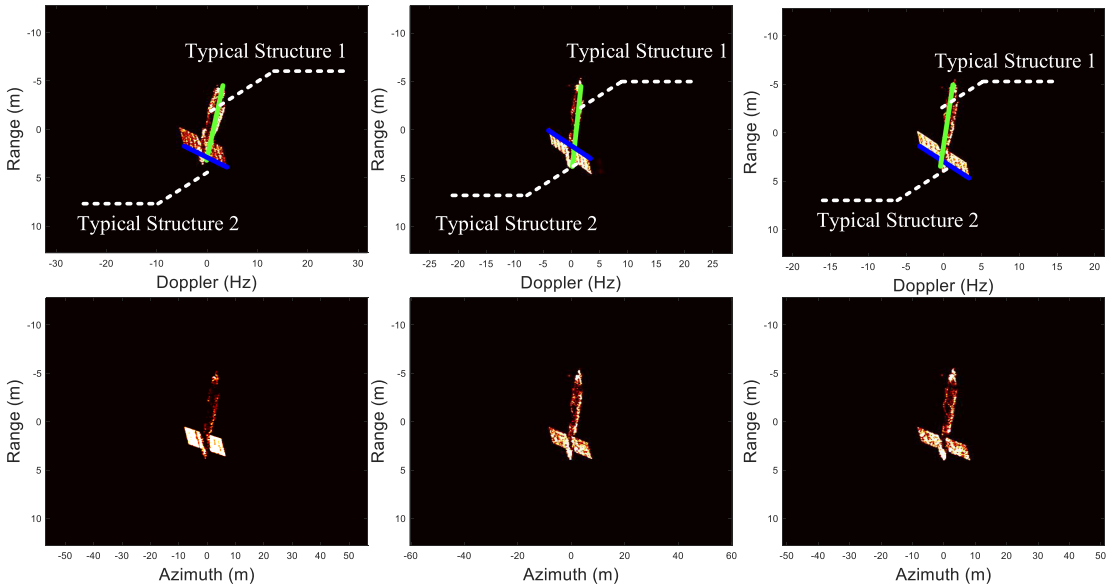

Fig. 8. Observation image feature extraction and matching with the simulation dataset in Scene 2. (First row: Feature extraction results of three frames in the observation image sequence; Second row: Image matching results with the simulation dataset via HMM decoding.).

TABLE III
Target Dynamic Parameter Estimation Results in Different Observation Conditions

Parameter	True value	Estimation result	Error
Scene 1			
The initial direction vector of the structure 1	(0.1168,0.3425,0.9322)	(0.1380,0.3077,0.9414)	2.43 degrees
The initial direction vector of the structure 2	(-0.8268,0.5536,-0.0998)	(-0.7983,0.5922,-0.1094)	2.78 degrees
The direction vector of the spin shaft	(0.8138,0.2962,-0.5000)	(-0.8166,-0.3369,0.4687)	2.95 degrees
Target spin speed	0.012 rad/s	0.013 rad/s	0.001 rad/s
Scene 2			
The initial direction vector of the structure 1	(-0.7125,0.5653,-0.4157)	(0.7075,-0.5827,0.3999)	1.39 degrees
The initial direction vector of the structure 2	(-0.2129,0.3903,0.8957)	(-0.1782,0.4304,0.8849)	3.10 degrees
The direction vector of the spin shaft	(0.1632,-0.0594,0.9848)	(0.1924,-0.0998,0.9762)	2.78 degrees
Target spin speed	0.014 rad/s	0.013 rad/s	0.001 rad/s

that of the existing algorithm in [27]. In [27], the projection lengths of target structures in an ISAR image sequence are used to estimate the attitude parameters of attitude-stabled satellites.

In the first comparison experiment, its estimation results for an attitude-stable target are compared with those of the proposed algorithm in the same observation condition. From the numerical comparison listed in Table IV, the estimation accuracy of these two methods all arrives at 3-degree level. However, when the target spins, the existing algorithm fails in the second comparison experiment, shown in Table V. Because the uncertain spin motion makes it difficult to solve target attitude parameters with wrong image scaling information. By contrast, the proposed algorithm works with the support from the generated image feature dataset due to the additional spin optimization. The estimation results confirm its progress on handling the dynamic estimation of spin satellites in the observation scene through the single ISAR device. Besides, only the prior 3-D model and observation geometry are required additionally, which can be ensured in most observation tasks.

D. Discussion of the Experiment Results

From the previous experiments, the effectiveness of the proposed algorithm is confirmed and its superiority also illustrated by the comparison with the existing method. According to the prior model and observation information, the relationship between the target dynamic parameters and the observed image feature sequence is mathematically derived in the proposed algorithm. In this way, target instantaneous attitude is acquired after the state sequence decoding and spin parameter optimization. However, some limitations

TABLE IV
Target Attitude Estimation Results for an Attitude-Stable Target

Parameter	True value	Estimation result	Error
The existing algorithm			
The direction vector of the structure 1	(0.8007,0.4314,-0.4157)	(-0.8058,-0.4123,0.4252)	1.26 degrees
The direction vector of the structure 2	(-0.1046,0.7839,0.6119)	(-0.0789,0.7863,0.6128)	1.48 degrees
The proposed algorithm			
The direction vector of the structure 1	(0.8007,0.4314,-0.4157)	(-0.7889,-0.4562,0.4116)	1.59 degrees
The direction vector of the structure 2	(-0.1046,0.7839,0.6119)	(-0.0799,0.7999,0.5948)	1.95 degrees

TABLE V
Target Attitude Estimation Results for a Spin Target

Parameter	True value	Estimation result	Error
The existing algorithm			
The initial direction vector of the structure 1	(0.8007,0.4314,-0.4157)	(-0.4708,0.7463,0.4705)	104.52 degrees
The initial direction vector of the structure 2	(-0.1046,0.7839,0.6119)	(0.8809,0.4270,0.2041)	68.44 degrees
The direction vector of the spin shaft	(0.3830,-0.3214,0.8660)	-	-
Target spin speed	0.015 rad/s	-	-
The proposed algorithm			
The initial direction vector of the structure 1	(0.8007,0.4314,-0.4157))	(-0.8008,-0.4221,0.4249)	0.75 degrees
The initial direction vector of the structure 2	(-0.1046,0.7839,0.6119)	(-0.0779,0.7769,0.6248)	1.75 degrees
The direction vector of the spin shaft	(0.3830,-0.3214,0.8660)	(0.3785,-0.3160,0.8700)	0.47 degrees
Target spin speed	0.015 rad/s	0.016 rad/s	0.001 rad/s

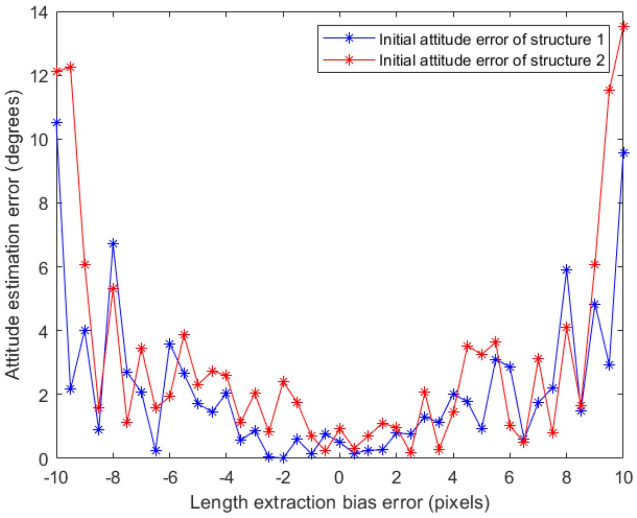

Fig. 9. Estimation error curve of the proposed method in different feature extraction conditions.

might affect the performance of proposed algorithm in real applications.

First, the segment interval of observation view restricts the estimation accuracy of target state parameters. As the parameter optimizations (21) and (22) are based on the decoded state sequence, the smaller segment interval in the all-view sampling would get finer projection feature expression. However, coupled with the decrease of segment interval, the number of potential states rapidly increases, leading the difficulty of training the HMM parameters. The balance between these two factors should be considered in the real applications. After the state elimination mentioned in Section.IV, the model of hundred-level hidden state is acceptable for most cases. Another way is to use machine learning algorithms, such as long short-term memory and recurrent neural network, replacing the HMM in decoding processing, which will be further investigated in our future work. Besides, at the current stage, the proposed algorithm is only applied to those targets spinning around a fixed shaft. As for more complicated on-orbit motion, more *priori* information should be provided to build the target spin parameter optimization. But it is still a challenge to make an explicit expression of target motion when targets tumble on the orbit.

VI. CONCLUSION

In this article, an approach was presented to achieve the dynamic estimation of spin satellites by interpreting single-station ISAR images. The complex high-dimension spin parameter estimation is split into sequential attitude matching and spin parameter optimization. With the accommodation of Viterbi algorithm and PSO algorithm, these two

subproblems are solved, respectively. The simulation experiment results illustrate the feasibility of the proposed algorithm. Compared with the existing methods, the proposed method makes the progress on the satellite monitoring with single-station radar sensor, which has a potential capacity for guiding resource allocation of a certain ground-based ISAR observation network in real applications.

ACKNOWLEDGMENT

The authors would like to thank the anonymous reviewers for their valuable comments to improve the article quality.

REFERENCES

[1] G. Kirchner, W. Hausleitner, and E. Cristea
Ajisai spin parameter determination using Graz kilohertz satellite laser ranging data
IEEE Trans. Geosci. Remote Sens., vol. 45, no. 1, pp. 201–205, Jan. 2007.

[2] D. Kucharski *et al.*
Attitude and spin period of space debris Envisat measured by satellite laser ranging
IEEE Trans. Geosci. Remote Sens., vol. 52, no. 12, pp. 7651–7657, Dec. 2014.

[3] N. Koshkin *et al.*
Ajisai spin-axis precession and rotation-period variations from photometric observations
Adv. Space Res., vol. 60, no. 7, pp. 1389–1399, 2017.

[4] N. Koshkin *et al.*
Remote sensing of the EnviSat and Cbers-2B satellites rotation around the centre of mass by photometry
Adv. Space Res., vol. 58, no. 3, pp. 358–371, 2016.

[5] N. O. Gmez and S. J. Walker
Earths gravity gradient and Eddy currents effects on the rotational dynamics of space debris objects: Envisat case study
Adv. Space Res., vol. 56, no. 3, pp. 494–508, 2015.

[6] H. Y. Lin and C. Y. Zhao
An estimation of Envisats rotational state accounting for the precession of its rotational axis caused by gravity gradient torque
Adv. Space Res., vol. 61, no. 1, pp. 182–188, 2018.

[7] S. Lemmens, H. Krag, and J. Rosebrock
Radar mappings for attitude analysis of objects in orbit
In *Proc. 6th Eur. Conf. Space Debris*, 2013, pp. 20–24.

[8] S. Lemmens and H. Krag
Sensitivity of automated attitude determination form ISAR radar mappings
In *Proc. Adv. Maui Opt. Space Surveill. Technol. Conf.*, 2013, pp. 1–12.

[9] M. Avils *et al.*
Automated attitude estimation from ISAR images
In *Proc. 7th Eur. Conf. Space Debris*, 2017, pp. 1–13.

[10] F. Terui, H. Kamimura, and I. Ninshidas
Motion estimation to a failed satellite on orbit using stereo vision and 3D model matching
In *Proc. 9th Int. Conf. Control, Autom., Robot. Vis.*, 2006, pp. 1–8.

[11] S. Segal, A. Carmi,, and P. Gurfil
Stereovision-based estimation of relative dynamics between noncooperative satellites: Theory and experiments
IEEE Trans. Control Syst. Technol., vol. 22, no. 2, pp. 568–584, Mar. 2014.

[12] J. Peng *et al.*
Pose measurement and motion estimation of space noncooperative targets based on laser radar and stereo-vision fusion
IEEE Sensors J., vol. 19, no. 8, pp. 3008–3019, Apr. 2019.

[13] K. Suwa, T. Wakayama, and M. Iwamoto
Three-dimensional target geometry and target motion estimation method using multistatic ISAR movies and its performance
IEEE Trans. Geosci. Remote Sens., vol. 49, no. 6, pp. 2361–2373, Jun. 2011.

[14] J. Rosebrock
Absolute attitude from monostatic radar measurements of rotating objects
IEEE Trans. Geosci. Remote Sens., vol. 49, no. 10, pp. 3737–3744, Oct. 2011.

[15] M. Martorella, D. Stagliano, and F. Salvetti
3D interferometric ISAR imaging of noncooperative targets
IEEE Trans. Aerosp. Electron. Syst., vol. 50, no. 4, pp. 3102–3114, Oct. 2014.

[16] Y. J. Zhou, L. Zhang, and Y. H. Cao
Dynamic estimation of spin spacecraft based on multiple-station ISAR images
IEEE Trans. Geosci. Remote Sens., vol. 58, no. 4, pp. 2977–2989, Apr. 2020.

[17] Y. J. Zhou *et al.*
Optical-and-radar image fusion for dynamic estimation of spin satellites
IEEE Trans. Image Process., vol. 29, no. 1, pp. 2963–2976, Jan. 2020.

[18] Y. J. Zhou *et al.*
Dynamic analysis of spin satellites through the quadratic phase estimation in multiple-station radar images
IEEE Trans. Comput. Imag., vol. 6, pp. 894–907, 2020.

[19] J. Cai *et al.*
Automatic target recognition based on alignments of three-dimensional interferometric ISAR images and CAD models
IEEE Trans. Aerosp. Electron. Syst., vol. 56, no. 6, pp. 4872–4888, Dec. 2020.

[20] L. Rabiner and J. Biinghwang
An introduction to hidden Markov models
IEEE ASSP Mag., vol. 3, no. 1, pp. 4–16, Jan. 1986.

[21] Z. Ghahramani
An introduction to hidden Markov models and Bayesian networks
Hidden Markov Models: Appl. Comput. Vis., vol. 1, pp. 9–41, 2001.

[22] A. J. Viterbi
Error bounds for convolutional codes and an asymptotically optimum decoding algorithm
IEEE Trans. Inf. Theory, vol. 13, no. 2, pp. 260–269, Apr. 1967.

[23] J. Li, W. Pedrycz, and I. Jamal
Multivariate time series anomaly detection: A framework of hidden Markov Models
Appl. Soft Comput., vol. 60, pp. 229–240, 2017.

[24] J. T. Mayhan *et al.*
High resolution 3D snapshot ISAR imaging and feature extraction
IEEE Trans. Aerosp. Electron. Syst., vol. 37, no. 2, pp. 630–642, Apr. 2001.

[25] G. Ettinger and W. Snyder
Model-based fusion of multi-look SAR for ATR
Proc. SPIE, vol. 4727, pp. 277–289, 2002.

[26] Z. Bao, M. Xing, and T. Wang
Radar Imaging Technology. Beijing, China: Publishing House Electronics Industry, 2005, pp. 24–40.

[27] Y. J. Zhou *et al.*
Attitude estimation and geometry reconstruction of satellite targets based on ISAR image sequence interpretation
IEEE Trans. Aerosp. Electron. Syst., vol. 55 no. 4, pp. 1698–1711, Aug. 2019.

[28] C. R. Gonzalesz and E. Richard
Digital Image Processing Beijing, China: Publishing House of Electronics Industry, 2007, pp. 432–435.

[29] S. Deans
The Radon Transform and Some of Its Applications. North Chelmsford, MA, USA: Courier Corporation, 2007.

[30] X. Li, M. Parizeau, and R. Plamondon
Training hidden Markov models with multiple observations—A combinatorial method
IEEE Trans. Pattern Anal. Mach. Intell., vol. 22, no. 4, pp. 371–377, Apr. 2000.

[31] P. M. Baggenstoss
A modified Baum–Welch algorithm for hidden Markov models with multiple observation spaces
IEEE Trans. Speech Audio Process., vol. 9, no. 4, pp. 411–416, May 2001.

[32] J. Kennedy and R. Eberhart
Particle swarm optimization
In *Proc. IEEE Int. Conf. Neural Netw.*, 2002, pp. 1942–1948.

[33] B. Riwanto
Particle swarm optimization with rotation axis fitting for magnetometer calibration
IEEE Trans. Aerosp. Electron. Syst., vol. 53, no. 2, pp. 1009–1022, Apr. 2017.

[34] F. Angel, A. Omar, and G. Jesus
Facet model of moving targets for ISAR imaging and radar back-scattering simulation
IEEE Trans. Aerosp. Electron. Syst., vol. 46, no. 3, pp. 1455–1467, Jul. 2010.

[35] L. Zhang *et al.*
Achieving higher resolution ISAR imaging with limited pulses via compressed sampling
IEEE Geosci. Remote Sens. Lett., vol. 6, no. 3, pp. 567–571, Jul. 2009.

[36] X. Bai *et al.*
High resolution ISAR imaging of targets with rotating parts
IEEE Trans. Aerosp. Electron. Syst., vol. 47 no. 4, pp. 2530–2543, Oct. 2011.

Yejian Zhou was born in Zhejiang Province, China, in 1993. He received the B.S. degree in electronic engineering and the Ph.D. degree in signal processing from Xidian University, Xi'an, China, in 2015 and 2020, respectively.

He was a Visiting Ph.D. student with the Department of Urban Planning and Environment, KTH Royal Institute of Technology, Stockholm, Sweden, from September 2019 to August 2020. He is currently an Assistant Professor with College of Information Engineering, Zhejiang University of Technology, Hangzhou, China. His research interests include ISAR imaging and image interpretation.

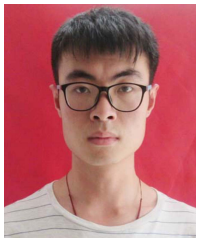

Shaopeng Wei was born in Shandong Province, China, in 1994. He received the B.S. degree in electronic engineering, in 2017, from Xidian University, Xi'an, China, where he is currently working toward the Ph.D. degree in signal processing with the National laboratory of Radar Signal Processing.

His research interests are radar signal processing and radar imaging.

Lei Zhang was born in Zhejiang Province, China, in 1984. He received the Ph.D degree in signal processing from Xidian University, Xi'an, China, in 2012.

He is currently working as a Professor with the School of Electronics and Communication Engineering, Sun Yat-Sen University (Shenzhen Campus), Guangzhou, Shenzhen, China. His research interests are radar imaging (SAR/ISAR) and motion compensation.

Wenan Zhang was born in Zhejiang Province, China, in 1982. He received the B.S. degree in automation and the Ph.D. degree in control theory and control engineering from the Zhejiang University of Technology, Hangzhou, China, in 2004 and 2010, respectively.

Since 2020, he has been with the Zhejiang University of Technology, where he is currently a Professor with the Department of Automation. He was a Senior Research Associate with the Department of Manufacturing Engineering and Engineering Management, City University of Hong Kong, Hong Kong, from 2010 to 2011. His research interests include multisensor information fusion estimation, and robotics.

Dr. Zhang was the recipient of the Alexander von Humboldt Fellowship, in 2011. He has been a Subject Editor for *Optimal Control Applications and Methods*, since September 2016.

Yan Ma was born in Shandong Province, China, in 1977. He received the M.S. degree in signal processing from Beijing Institute of Tracking Telemetry and Telecommunication, Beijing, China, in 2002.

He is currently a Research Fellow with Beijing Institute of Tracking Telemetry and Telecommunication. His research interests include signal processing and target recognition.